Photocatalyst–mediator interface modification by surface-metal cations of a dye-sensitized H_2 evolution photocatalyst

Nobutaka Yoshimura,[a] *Masaki Yoshida,*[a] *Masako Kato,*[a,b] *Atsushi Kobayashi**[a]

[a]Department of Chemistry, Faculty of Science, Hokkaido University, North-10 West-8, Kita-ku, Sapporo 060-0810, Japan

[b]Department of Applied Chemistry for Environment, School of Biological and Environmental Sciences, Kwansei Gakuin University, 2-1 Gakuen, Sanda, Hyogo 669-1337, Japan.

ABSTRACT: To develop a highly active H_2 evolving dye-sensitized photocatalysts (DSPs) applicable for Z-scheme water splitting, we synthesized a series of Ru(II)-dye-double-layered DSPs, M'-**RuCP^6**-Zr-**RuP^6**@Pt-TiO_2 (**M'-DSP**) with different surface-bound metal cations (M' = Fe^{2+}, Y^{3+}, Zr^{4+}, Hf^{4+}, and Bi^{3+}). In 0.5 M KI aqueous solution, the photocatalytic H_2 evolution activity under blue light irradiation (λ = 460±15 nm) increased in the following order: non-metal-modified DSP, **H^+-DSP** (turn over number for 6 h irradiation = 35.2) < **Fe^{2+}-DSP** (54.9) ≅ **Bi^{3+}-DSP** (55.2) < **Hf^{4+}-DSP** (65.5) ≅ **Zr^{4+}-DSP** (68.3) ≅ **Y^{3+}-DSP** (71.5), suggesting that the redox-inactive and highly-charged metal cations tend to improve the electron donation from the iodide electron mediator. On the other hand, DSPs having heavy metal cations, **Hf^{4+}-DSP** (18.4) and **Bi^{3+}-DSP** (16.6) exhibited better activity under green light irradiation (λ = 530±15 nm) than **Zr^{4+}-DSP** (15.7) and **H^+-DSP** (7.80), implying the contribution of heavy atom effect of the surface-bound metal cation to partially allow the spin-forbidden metal-to-ligand charge-transfer excitation.

Introduction

Photocatalytic solar water splitting is a desirable reaction for solving global energy and environmental issues.[1-5] Since the discovery of the Honda-Fujishima effect,[6] many semiconductor photocatalysts have been developed. In particular, the construction of a Z-scheme system by combining H_2 and O_2 evolving photocatalysts (OEP and HEP) has attracted considerable attention as a useful strategy to utilize visible light and ensure a sufficiently large driving force for water splitting and electron transfer reactions.[7-10] For example, in 2016, Domen *et al.* reported a Z-scheme photocatalyst composed of La- and Rh-codoped $SrTiO_3$ and Mo-doped $BiVO_4$—as the H_2 and O_2 evolving photocatalysts, respectively—on a gold layer, which exhibited 1.1% solar-to-hydrogen (STH) energy conversion efficiency and over 30% apparent quantum efficiency (AQY) at 419 nm.[11] However, further improvement of both the STH and AQY is still necessary for practical application. To achieve this, two targets must be reached: The first is to utilize the longer wavelength range to improve the STH energy conversion efficiency[4,12-13] and the second is to achieve one-way electron transfer from the OEP to HEP *via* an electron mediator.[14-16]

Dye-sensitization is a well-known and extensively studied technique to overcome the weak visible light absorption of a semiconductor substrates.[17-29] Abe *et al*. reported on a Z-scheme water-splitting photocatalyst composed of coumarin-dye-sensitized $Pt/H_4Nb_6O_{17}$ as the HEP and IrO_2-Pt/WO_3 as the OEP.[30] A remarkably high AQY (2.4% at 420 nm) was achieved by a recently developed Z-scheme system consisting of a Ru(II)-dye-sensitized Al_2O_3 cluster-deposited/$Pt/HCa_2Nb_3O_{10}$ as the HEP.[31] Although the AQY and STH values of dye-sensitized photocatalysts (DSPs) are still lower than those of their metal-oxide-based counterparts, the dye-sensitization technique offers a unique advantage. Indeed, further modification at the dye-

semiconductor interface is possible by co-absorption and/or multilayering of functional molecules, as evidenced by recent studies in dye-sensitized solar (DSSCs) and electrochemical (DSPEC) cells.[32-35] Meyer *et al.* demonstrated one-directional energy transfer in a bilayer film composed of two different Ru(II) dyes.[36-40] Hanson *et al.* reported that the lifetime of the charge-separated state can be controlled by introducing an organic spacer molecule into the dye–semiconductor interface with various metal cation linkages.[41-44] Further, several research groups have reported that the host–guest interaction is useful for softly immobilizing dyes and catalyst molecules on the semiconductor surface.[45-49] However, literature on the further modification of the dye–semiconductor interface in the field of DSP for water splitting remains limited.

In this context, we previously reported on a DSP nanoparticle consisting of a Pt-cocatalyst-loaded TiO_2 nanoparticle covered by a bilayer film formed from two Ru(II) dyes with Zr^{4+} cations—Zr-**RuCP^6**-Zr-**RuP^6**@Pt-TiO_2 (**Zr^{4+}-DSP**, **RuCP^6** = $[Ru(mpbpy)_3]^{10-}$, where **RuP^6** = $[Ru(pbpy)_3]^{10-}$, H_4mpbpy = 2,2′-bipyridine-4,4′-bis(methane-phosphonic acid), and H_4pbpy = 2,2′-bipyridine-4,4′-bis(phosphonic acid)}. The Zr^{4+} cations bound by the outer-surface phosphonate groups of the **RuCP^6** dye played a key role in the dye regeneration by the iodide redox-reversible electron donor as in the case of DSSCs,[43] leading to superior photocatalytic H_2 evolution activity compared to that observed in the absence of the surface Zr^{4+} cation.[50-54] These results motivated us to improve the outer surface structure by changing the surface Zr^{4+} cations to other metal cations. Such an approach should be valuable not only to enhance the photocatalytic activity, but also to clarify the versatility of this surface-metal cation modification method for one-directional electron transfer at the photocatalyst–mediator interface. Several DSSC studies revealed that metal ion coordination to the functional groups of dye molecule certainly effects on the charge-separation/recombination processes at the photoelectrode-

mediator interface, leading to the improved DSSC performance.[38-40,55] Herein, we report the preparation, characterization, and photocatalytic H_2 evolution reactions of surface-metal-replaced DSP nanoparticles—X'-**RuCP^6**-Zr-**RuP^6**@Pt-TiO_2 (**X'-DSP**; Scheme 1 and Scheme S1; X' = H^+, Sr^{2+}, Fe^{2+}, Y^{3+}, Zr^{4+}, Hf^{4+}, and Bi^{3+}). The replacing surface-metal cation from Zr^{4+} to Sr^{2+} or Y^{3+} having the same closed [Kr] electronic configuration should reveal the importance of ionic radius and formal charge. Hf^{4+} exhibiting similar chemical bonding nature to Zr^{4+} was selected to reveal the effect of heavy atom effect on the charge-separation process at the TiO^{2+}-dye-mediator interfaces. Further, the redox active metal cations Fe^{2+} and Bi^{3+} were also introduced to evaluate the importance of redox behavior of the surface metal cations that may promote the charge-separation. We demonstrate that five of the as-synthesized DSPs (X' = Fe^{2+}, Y^{3+}, Hf^{4+}, Bi^{3+}, and the previously synthesized Zr^{4+}) showed 1.6- to 2-fold higher photocatalytic activity than that of **H$^+$-DSP** without surface metal ions. Furthermore, the **X'-DSP**s comprising heavy metal cations (X' = Zr^{4+}, Hf^{4+}, and Bi^{3+}) maintained relatively high activities under green light irradiation (λ = 530±15 nm, 0.2~0.3% AQY), which only excited the lower band edge of the metal-to-ligand charge-transfer (^{1}MLCT) transition of the Ru dyes. These results suggest that dye multilayering and surface modification by metal cations are useful approaches for improving the reactivity with anionic electron donors and enhancing the photocatalytic activity under light irradiation at the absorption band edge region.

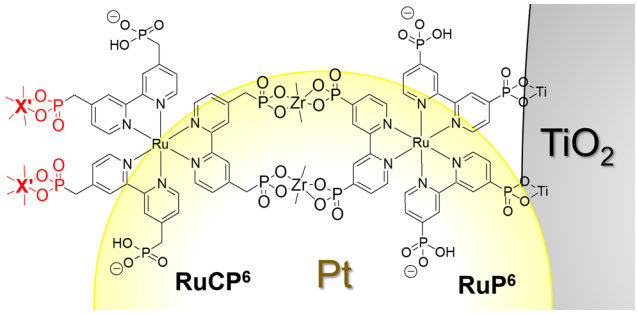

Scheme 1. Schematic surface structure of the X'-**RuCP^6**-Zr-**RuP^6**@Pt-TiO_2 nanoparticle (**X'-DSP**, X' = H^+, Sr^{2+}, Fe^{2+}, Y^{3+}, Zr^{4+} Hf^{4+}, and Bi^{3+}).

Experimental Section

Materials and Syntheses

Caution! *Although we did not encounter any difficulties, most of the chemicals used in this study are potentially harmful and should be used in small quantities and handled with care in a fume hood.* All the commercially available starting materials were used as received without further purification. TiO_2 nanoparticles (SSP-M, ~15 nm in diameter) were purchased from Sakai Chemical Industry Co., Ltd. (Sakai, Osaka, Japan) Pt-TiO_2 (1 wt%) was prepared using a previously reported photodeposition method.[56] The Ru(II) molecular photosensitizers (PSs; **RuCP^6** and **RuP^6**)[50,57] were synthesized using previously reported methods. $FeCl_2{\cdot}4H_2O$, $SrCl_2{\cdot}6H_2O$, $YCl_3{\cdot}6H_2O$, $ZrCl_2O{\cdot}8H_2O$, $HfCl_2O{\cdot}8H_2O$, and $BiCl_3$ were used as the starting materials for the immobilization of the outer metal ions.

Preparation of Ru(II)-dye-immobilized Pt-TiO_2 nanoparticles (X'-DSPs)

RuCP^{6}-Zr-**RuP^{6}**@Pt-TiO_2 (**H^{+}-DSP**) nanoparticles were synthesized with reference to our previous reports.[50,53] Immobilization of the outer metal ions was conducted by the same synthetic method as that of Zr^{4+}-**RuCP^{6}**-Zr-**RuP^{6}**@Pt-TiO_2 (**Zr^{4+}-DSP**), except for the use of other metal salts instead of $ZrCl_2O{\cdot}8H_2O$ as follows. 30 mg of **H^{+}-DSP** was added to 25 mM of $FeCl_2{\cdot}4H_2O$, $SrCl_2{\cdot}6H_2O$, $YCl_3{\cdot}6H_2O$, $ZrCl_2O{\cdot}8H_2O$, $HfCl_2O{\cdot}8H_2O$, or $BiCl_3$ MeOH solution (6 mL, about 50 eq. to the surface immobilized Ru(II) dye) and this suspension was stirred for 1 h at 298 K under dark. Then, the orange suspension was ultra-centrifugated (50,000 rpm, 20 min) and washed twice with small portions of MeOH. The precipitation was dried for a few days at 298~328 K to afford **X'-DSP**. The amount of Ru(II) dye immobilized on the Pt-TiO_2 nanoparticle surface was estimated using X-ray fluorescence (XRF) spectroscopy of the solid samples and UV-vis absorption spectroscopy of the supernatant solution (see Figure S1, Table S1, and the "Calculation of the amount of Ru(II) complex immobilized on the Pt-TiO_2 nanoparticles" section of the ESI). The loaded amounts of Pt cocatalyst on the Pt-TiO_2 nanoparticles were estimated from the XRF spectra to be 0.99 wt%.

Measurements

UV−vis absorption spectra were recorded on a Shimadzu UV-2400PC spectrophotometer and Hitachi U-3000 UV-vis spectrometer. Luminescence spectra were recorded on JASCO FP-6600 and FP-8600 spectrofluorometers at 298 K. Each sample solution was deoxygenated by N_2 bubbling for 30 min at 298 K. Energy-dispersive XRF spectra were recorded using a Bruker S2 PUMA analyzer at 298 K. Scanning electron microscope and energy dispersive X-ray spectroscopy (SEM-EDS) analysis was performed using Phenom World Phenom ProX scanning electron microscope (15 kV).

Photocatalytic water reduction reaction

Under dark conditions, an aqueous solution of KI (0.5 M) in hydrochloride (pH 2) containing Ru(II)-dye-immobilized nanoparticles (100 μM Ru(II) dye) was placed into an in-lab Schlenk flask-equipped quartz cell (volume, 265 mL) with a small magnetic stirring bar. Each sample flask was doubly sealed with rubber septum. This mixed solution was deoxygenated by bubbling with Ar for 1 h. The flask was then irradiated from the bottom using a blue {λ = 460 ± 15 nm; 70 mW; Opto Device Lab. Ltd., (Kumagaya, Saitama, Japan) OP6-4710HP2} or green (λ = 530 ± 15 nm; 40 mW; Opto Device Lab. Ltd., OP6-5310HP2) LED lamp (Figure S2 and Table S2) as peak top and edge of ^{1}MLCT absorption band of Ru(II) dye (Table S3). The temperature was maintained at 293 K using an in-lab aluminum water-cooling jacket with a water-circulating temperature controller {Eyela (Bunkyo-ku, Tokyo, Japan) CCA-1111}. The gas samples (0.6 mL) for each analysis were collected from the headspace using a gastight syringe {1 mL, Valco Instruments Co. Inc. (Houston, Texas, USA)}. The amount of evolved H_2 was determined using gas chromatography {Agilent (Santa Clara, California, USA) 490 Micro}. The turnover number and turnover frequency per Ru dye (PS TON and TOF, respectively) were estimated from the amount of evolved H_2, wherein two photoredox cycles of the Ru(II) PS are required to produce one H_2 molecule. Each photocatalytic H_2 evolution reaction was conducted thrice under the same conditions, and the average value with the standard deviation was reported. The detection limit of the gas chromatography analysis for H_2 gas in this study was 0.005 μmol. The AQY was calculated using the following equation I:

$$AQY = N_e/N_p = 2N_{H2}/ N_p \qquad (I)$$

where N_e represents the number of reacted electrons, N_{H2} is the number of evolved H_2 molecules, and N_p is the number of incident photons.

Results and Discussion

Characterization of the Ru(II)-dye-immobilized Pt-TiO_2 nanoparticles

Figure 1 shows the XRF spectra of the Ru(II)-dye-immobilized Pt-TiO_2 nanoparticles in the solid state at 298 K. As we previously reported,[50] Zr Kα and Ru Kα radiation originating from the bridging Zr^{4+} cations and Ru(II) dyes (**RuCP^6** and **RuP^6**) was clearly observed at the 15.7 and 19.2 keV regions, respectively, in addition to the Pt L and Ti K radiation originating from the Pt-TiO_2 nanoparticles. The Zr/Ru molecular ratio for **Zr^{4+}-DSP** was estimated from the radiation intensity ratio to be 2.2(1), which is approximately twice the estimated value for **H^+-DSP** (1.3(1), see Table S4). This result suggests that the **Zr^{4+}-DSP** nanoparticle was formed by binding of the Zr^{4+} ion with the phosphonate groups on the outer surface of **H^+-DSP**. For the **X'-DSPs** comprising the other metal cations (X' = Sr^{2+}, Fe^{2+}, Y^{3+}, Hf^{4+}, and Bi^{3+}) at the outer surface of **H^+-DSP**, the characteristic X-ray radiation assignable to the metal ions (Fe Kα; Sr Kα; Y Kα; Hf Lα and Lβ; and Bi Lα, Lβ, and Lγ) was observed. The peak intensities of the Zr Kα and Ru Kα radiation for all five **X'-DSPs** were almost comparable to those of **H^+-DSP**. Thus, we supposed that the metal ions were immobilized on the outer phosphonate groups of **RuCP^6** without substitution of the inner Zr^{4+} ions or desorption of the **RuCP^6** dye. In fact, the characteristic ^{1}MLCT absorption of **RuCP^6** dye was hardly observed in the UV-vis absorption spectrum of the 2nd Zr^{4+} loading solution (see Figure S3). The X'/Ru molecular ratio was estimated based on the intensity of the Kα or Lα radiation of the outer metal cation (Table S4) and decreased in the

order **Zr^{4+}-DSP** (X'/Ru = 0.9(1)) = **Hf^{4+}-DSP** (X'/ Ru = 0.9(1)) ≥ **Bi^{3+}-DSP** (X'/Ru = 0.7(1)) ≥ **Fe^{2+}-DSP** (X'/Ru = 0.5(1)) > **Y^{3+}-DSP** (X'/Ru = 0.1(1)) > **Sr^{2+}-DSP** (X'/Ru < 0.1). The estimated X'/Ru ratio tends to decrease with decreasing formal charge ($V_{X'}$) and absolute value of the hydration enthalpy (ΔH_{hyd}) of the outer metal cation (see Table S4, Table S5). Although additional experiments are necessary to make the conclusion about this trend, it may occur because the smaller $V_{X'}$ weakens the ionic bond between X' and the phosphonate, and the smaller ΔH_{hyd} causes rapid ligand exchange reaction of the X' cation. In fact, the Sr^{2+} ions with the smallest $V_{X'}$ and ΔH_{hyd} values examined in this work were easily desorbed from the nanoparticle surface of **Sr^{2+}-DSP** by immersion into a 0.5 M KCl aqueous solution for 1 h at 298 K (Figure S4). Specifically, metal ions with larger $V_{X'}$ and ΔH_{hyd} values, such as Hf^{4+}, can be tightly bound by the surface phosphonates even in highly polar aqueous solutions, and are suitable for the surface functionalization of nanoparticle photocatalysts. In addition, we also found that the loading amount of Zr^{4+} cation of **Zr^{4+}-DSP** hardly increased by twice repeating the immobilization reaction of Zr^{4+} in MeOH solution (Figure S5), suggesting that most of the surface phosphonate groups were bound to Zr^{4+}.

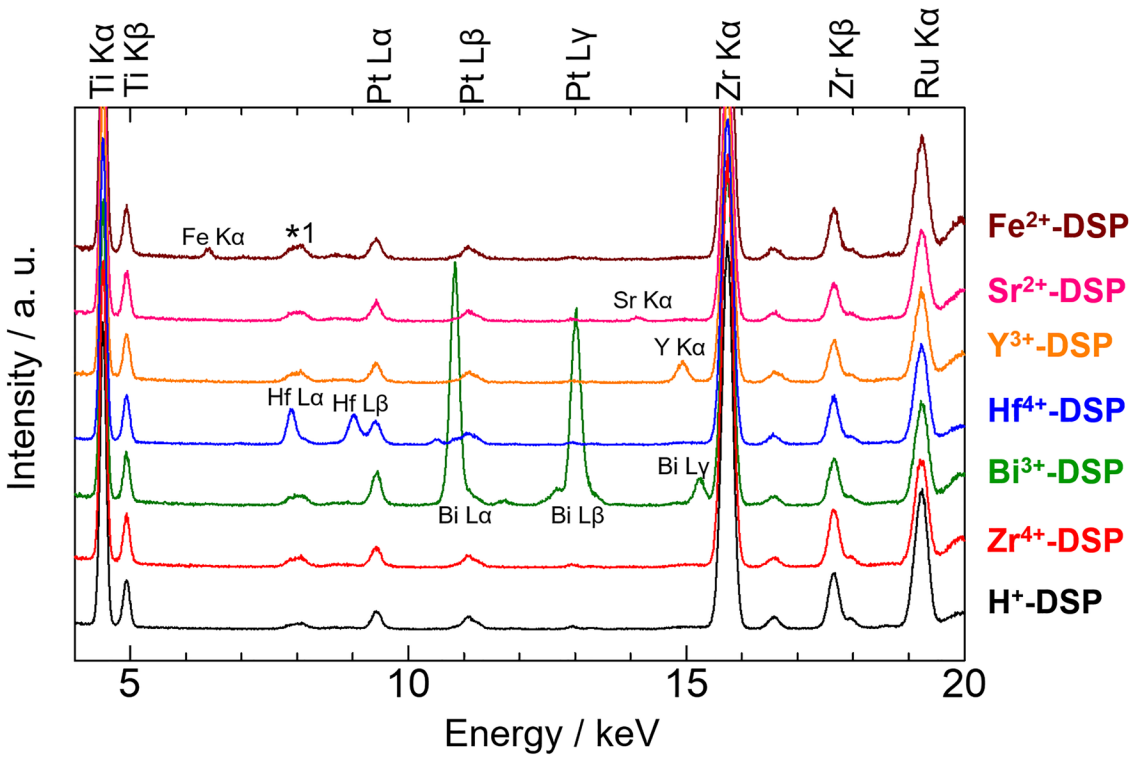

Figure 1. X-ray fluorescence (XRF) spectra of **X'-DSPs** in the solid state. All spectra were normalized using the Ti Kα peak. The peak marked as *1 is the background of the Cu sample holder.

Surface metal ion dependence

Figure 2 shows the results of the photocatalytic H_2 evolution reactions using **X'-DSPs** (X' = H^+, Fe^{2+}, Y^{3+}, Zr^{4+} Hf^{4+}, Bi^{3+}) nanoparticles in 0.5 M KI aqueous solution as the photocatalyst. The PS TON, PS TOF, and AQY are listed in Table 1. Note that the total amount of Ru(II) dye in each solution was constant (100 μM) and no hydrogen evolution was observed in the absence of Ru(II) dye, light, or electron donor (Table S6). The characteristic absorption bands of triiodide anion (I_3^-) was clearly observed in the UV-vis absorption spectra of the reaction solution after 6

h irradiation (Figure S6). The amount of I_3^- was estimated based on the molar absorption coefficient at 350 nm (about 14 μmol) to be comparable to that of H_2, indicating that the electron source of H_2 evolution is the iodide anions in the reaction solution. In addition, observed pH change from 2.0 to 2.4 in the reaction driven by **Zr^{4+}-DSP** suggest that the protons in the reaction solution were reduced photocatalytically to H_2. All metal-cation-immobilized **X'-DSPs** evolved at least 1.5 times more H_2 than did the **H^+-DSP**, suggesting a positive effect of metal ion coordination to the surface of the phosphonate groups on the photocatalytic H_2 evolution reaction. This result qualitatively agrees with the Hanson's works on the Ru(II)-dye-sensitized solar cells in which the open circuit voltage was improved by the surface-metal cation modification.[39] Although all metal-cation-immobilized **X'-DSPs** nanoparticles evolved comparable amounts of H_2, notable trends were observed, whereby the amounts of evolved H_2 with **Bi^{3+}-DSP** and **Fe^{2+}-DSP** were 20% less than those with **X'-DSPs** (X' = Zr^{4+}, Hf^{4+}, and Y^{3+}). The plausible reason may be the redox-active nature of these metal cations, wherein Bi^{3+} and Fe^{2+} have more positive reduction potentials than the oxidation potential of the photoexcited Ru(II)* dyes ($E(Bi^{3+}/Bi^{+}) = +0.20$ V vs. NHE, $E(Fe^{3+}/Fe^{2+}) = +0.77$ V vs. NHE, see Table S7) in addition to the energy transfer quenching by paramagnetic Fe^{2+} cation as reported in the literature.[39] These may induce the opposite electron/energy transfers from the outer **$RuCP^{6}$*** dye to the surface X' cation, leading to the lower photocatalytic activity. It is interesting to note that **Y^{3+}-DSP**, which has the largest X' ionic radius (Y^{3+}: 116 pm, Zr^{4+}: 98 pm, Hf^{4+}: 97 pm) with 10-times diluted X' cations on the surface than **Zr^{4+}-DSP**, exhibited near-identical activity as that of **Zr^{4+}-DSP**.

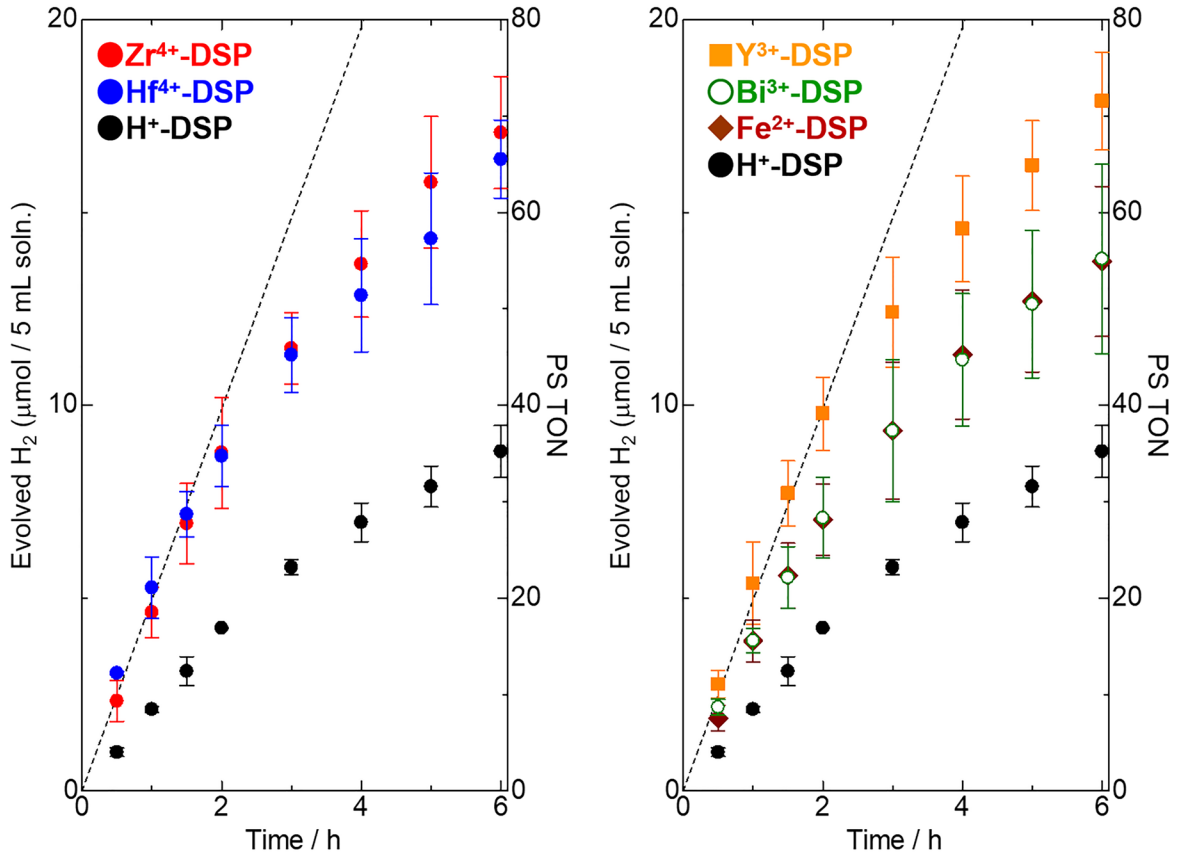

Figure 2. Photocatalytic H_2 evolution reactions driven by **X'-DSPs** in the presence of 100 μM Ru(II) dye and 0.5 M KI as the electron donor (initial pH = 2.0, λ = 460 ± 15 nm, 70 mW in total). Dashed line in each panel indicates AQY = 1%.

To clarify the interaction between **X'-DSP** and iodide mediator, the zeta (ζ) potentials in HCl aqueous solution (pH 2) with/without KI were evaluated (Table S8). In the HCl aqueous solution without iodide, all metal-cation-immobilized **X'-DSPs** showed an almost neutral ζ potential (–3.5 to +3.8 mV). On the other hand, in the presence of KI, the ζ potential of each metal-cation-immobilized **X'-DSPs** was negatively shifted (–7.6 to –13 mV). Considering that the comparable

zeta potential shift was also observed for the Pt-TiO_2 nanoparticle without Ru(II) dyes (+27 to +12 mV) and the **RuP^6**-sensitized Pt-TiO_2 nanoparticle (**RuP^6**@Pt-TiO_2, from –4.6 to –14 mV), the positively charged TiO_2 surface in the acidic pH condition may attract iodide anions electrostatically even after the loading of negatively charged Ru(II) dyes. This zeta potential shift by adding KI was negligible only for Zr-**RuP^6**@Pt-TiO_2, implying that not only the bare TiO_2 surface but also the 2nd-outer **RuCP^6** dye layer with the surface X' cations may act as the interaction sites for iodide attraction. The photocatalytic activity of all the samples gradually decreased; for example, the AQY at the initial 1 h of reaction (*i*AQY) of **Hf^{4+}-DSP** was 1.09%, whereas the average AQY after 6 h was approximately reduced by half (0.562%). The SEM image of **Hf^{4+}-DSP** was hardly changed after 6 h reaction, and the L and M radiations of Ru and Hf elements were clearly observed at 2.6 and 1.6 keV, respectively in the EDS spectra (Figure S7), suggesting that **Hf^{4+}-DSP** hardly decomposed during the reaction. Thus, the origin of gradual decrease of photocatalytic activity is because triiodide, generated as the oxidation product of H_2 evolution, exhibited moderate light absorptivity (1110 M^{-1} cm^{-1} at 460 nm) and disturbed the light absorption of the Ru(II) PSs (Figure S8).

Table 1. Results of the photocatalytic H_2 evolution experiments of **X'-DSPs** in 0.5 KI aqueous solution.

X'	λ_{ex} (nm)	H_2[a] (μmol) (0–6 h)	PS TON[a] (0–3 h)	PS TON[a] (0–6 h)	PS initial TOF[a]	AQY[a] (%) (0–6 h)	*i*AQY[a] (%) (0–1 h)
H^+	460 ± 15	8.80±0.7	23.2	35.2	8.47	0.302	0.436
Y^{3+}	460 ± 15	17.9±1.3	49.6	71.5	21.5	0.614	1.11
Zr^{4+}	460 ± 15	17.1±1.5	45.9	68.3	18.5	0.587	0.952
Hf^{4+}	460 ± 15	16.4±1.0	45.2	65.5	21.1	0.562	1.09
Bi^{3+}	460 ± 15	13.8±2.5	37.4	55.2	15.6	0.474	0.803
Fe^{2+}	460 ± 15	13.7±1.9	37.4	54.9	15.5	0.470	0.798
H^+	530 ± 15	1.95±0.47	5.06	7.80	2.01	0.102	0.157
Zr^{4+}	530 ± 15	3.93±0.27	9.95	15.7	4.30	0.205	0.337
Hf^{4+}	530 ± 15	4.61±0.08	11.8	18.4	4.41	0.241	0.345
Bi^{3+}	530 ± 15	4.14±0.07	9.79	16.6	2.81	0.216	0.220

[a]Reaction conditions: [Ru-PS] = 100 μM in total, [KI] = 0.5 M, HCl aqueous solution (pH 2), λ_{ex} = 460 ± 15 nm (70 mW in total) or 530 ± 15 nm (40 mW in total). The reaction solution was purged with bubbling Ar for 1 h before light irradiation. The numerical values represent the averages of more than three experiments. Definitions: PS, photosensitizer; TON, turnover number; TOF, turnover frequency; AQY, apparent quantum yield for total 6 h reaction; *i*AQY, AQY at the initial 1h of reaction.

Excitation wavelength dependence

From the viewpoint of the effective utilization of solar light, the utilization of longer-wavelength light for photocatalytic H_2 evolution is crucial. The photocatalytic activities of **Zr^{4+}-DSP**, **Hf^{4+}-DSP**, and **Bi^{3+}-DSP** under green light excitation (λ = 530 ±15 nm) were next investigated. Although [Ru(bpy)$_3$]-type dyes are well-known PSs for blue light excitation because of their

strong ^{1}MLCT absorption character at approximately 460 nm, both **RuCP^6** and **RuP^6** exhibit weak MLCT absorption shoulders up to approximately 590 nm (molar absorption coefficient, ε is 1540 and 1910 M^{-1} cm^{-1} at 530 nm, respectively. See Figure S2 and Table S3). We thus expected that heavier surface X' cations, such as Hf^{4+} and Bi^{3+}, might partially allow spin-forbidden ^{3}MLCT excitation by the strong heavy-atom effect *via* the coordination bonds with the phosphonate group. In addition, light shielding by triiodide should be suppressed under green light irradiation because of its smaller ε at 530 nm (152 M^{-1} cm^{-1}) than at 460 nm (1110 M^{-1} cm^{-1}; see Figure S8 and Table S9).

The results of the photocatalytic H_2 evolution reactions under green light irradiation are shown in Figure 3, while the estimated PS TON, TOF, and AQY values are listed in Table 1. Even under green light irradiation, the estimated TON for all cases exceeded one, indicating that H_2 evolution from iodide occurred photocatalytically. The amount of H_2 produced after 6 h of green light irradiation was smaller than that under blue light irradiation in all cases, because of the lower ε of the Ru PSs for green light. The comparable TON value of **Hf^{4+}-DSP** to that under blue light irradiation (TON = 45.2 for 3 h) was achieved by long-term photocatalytic reaction for 20 h (TON ~ 40, see Figure S9). A notable difference between the metal-cation-immobilized **X'-DSPs** and **H^+-DSP** was observed. Under blue light irradiation, the PS TON of metal-cation-immobilized **X'-DSPs** after 6 h irradiation was 1.6–1.94 times higher than that of **H^+-DSP**, while the difference under green light illumination was more pronounced (e.g., 1.9–2.4 times larger PS TON for metal-cation-immobilized **X'-DSPs**). The electron transfer from the redox-reversible iodide donor to the one-electron oxidized Ru(III) dye should be the important step in these photocatalytic H_2 evolutions, because the back electron transfer to the iodide radical ($I^\bullet$, $E(I^\bullet/I^-)$ = 1.33 V vs NHE) from the regenerated Ru(II) dye ($E(Ru^{III}/Ru^{II})$ = 1.12 V for **RuCP^6**) possibly

occurs just after the dye regeneration.[58-59] The photoexcitation frequency of Ru dyes under green light irradiation (λ = 530 nm, 40 mW) must be lower than that under blue light (λ = 460 nm, 70 mW) because of the lower ε of the Ru dye and lower light intensity of the LED light source. Hence, the direct coupling between two iodine radicals to form a stable and weaker oxidant iodine molecule (I_2, $E(I_2/I^-)$ = 0.54 V) should be negligible. The possible reaction in this case would be bond formation between the iodine radical $I^\bullet$ and iodide anion I^- to form a diiodide radical anion ($I_2^{\bullet-}$, $E(I_2^{\bullet-}/I^-)$ = 1.03 V), which should be favorable at high I^- concentrations. Thus, the superior activity of metal-cation-immobilized **X'-DSPs** compared to that of **H^+-DSP** was attributed to the more effective interaction between the iodide and surface of metal-cation-immobilized **X'-DSPs** than that with **H^+-DSP**. This leads to more efficient dye regeneration by iodide, even at the lower photoexcitation frequency from green light irradiation.

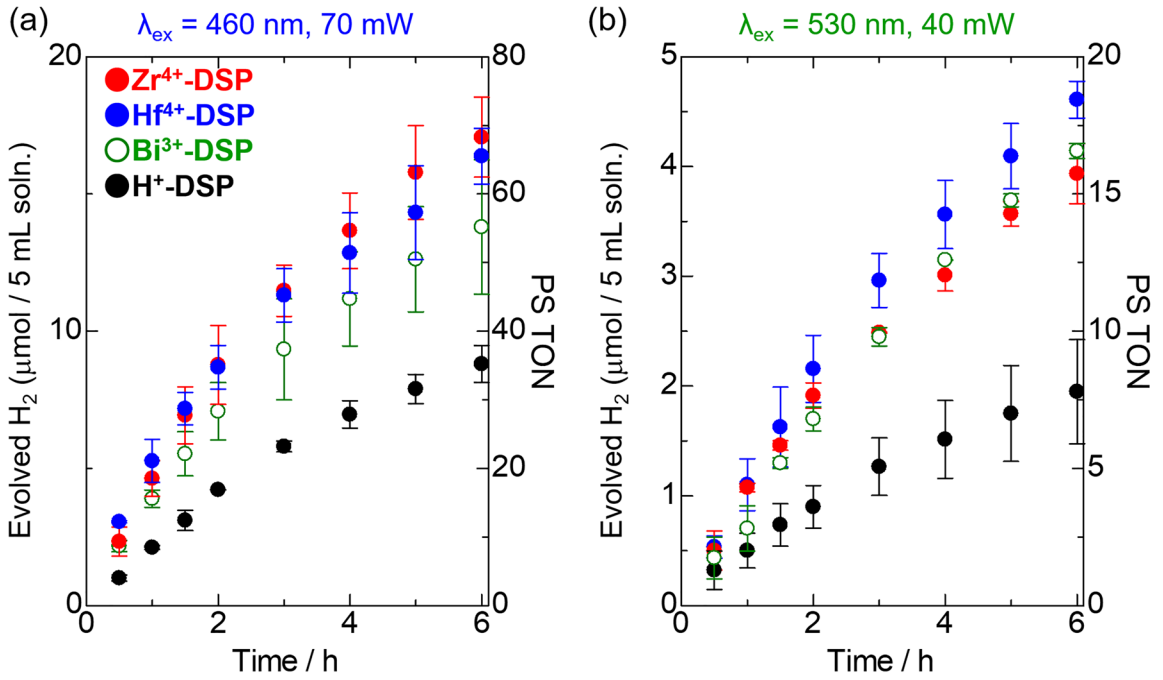

Figure 3. (a) Photocatalytic H_2 evolution reactions driven by **X'-DSPs** under blue light (460 ± 15 nm, 70 mW) or (b) green light (530 ± 15 nm, 40 mW in total) irradiation in the presence of 100 μM Ru(II) dye and 0.5 M KI as the electron donor (initial pH = 2.0).

The molar absorption coefficients of **RuCP**[6] and **RuP**[6] at 530 nm were estimated to be 1540 and 1950 M^{-1} cm^{-1}, respectively, by UV-vis absorption spectroscopy in dilute HCl aqueous solution (pH 2, Figure S2 and Figure S10). The total amount of Ru(II) dye used in each photocatalytic H_2 evolution was 100 μM, so that the absorbance at 530 nm was estimated to be 0.17, based on the Lambert-Beer law in which the effects of dye immobilization on Pt-TiO_2, the crosslinking Zr ions, and surface metal ions were ignored. This value indicates that only 33% of irradiated green light was absorbed by the Ru(II) dyes. The absorbance of the reaction solution at 460 nm was similarly estimated to be approximately 1.6, suggesting that most of the irradiated blue light (~97%) was absorbed by the Ru(II) dyes. Thus, the decrease in AQY of **Zr^{4+}-DSP** at 530 nm

irradiation to a third of that at 460 nm irradiation was primarily due to the smaller absorptivity. This implies that the irradiation wavelength dependence of the charge separation efficiency at the semiconductor–dye and dye–mediator interfaces of **Zr^{4+}-DSP** should be negligible.

Interestingly, the amounts of evolved H_2 for **Bi^{3+}-DSP** and **Hf^{4+}-DSP** after 6 h of green light irradiation were slightly larger than that of **Zr^{4+}-DSP**. The reverse trend was observed for blue light irradiation, wherein **Bi^{3+}-DSP** and **Hf^{4+}-DSP** respectively evolved slightly lower and comparable amounts of H_2 compared to that evolved by **Zr^{4+}-DSP**. The electrostatic interaction between the photocatalyst nanoparticle and iodide electron donor should be independent of the light source and was roughly estimated to be comparable among the three photocatalysts, as suggested by their zeta potentials (Table S8). One possible origin of the slightly higher activity of **Bi^{3+}-DSP** and **Hf^{4+}-DSP** than that of **Zr^{4+}-DSP** under green light illumination may be due to the different contributions of the spin-forbidden ^{3}MLCT transition—this could be partially allowed by the stronger heavy atom effect of the surface-immobilized Hf^{4+} and Bi^{3+} cations compared to that of Zr^{4+}. Unfortunately, a negligible difference was observed in the UV-vis diffuse reflectance spectra in the solid state (Figure S10), probably because of the light scattering of the TiO_2 nanoparticles. Further investigations to clarify the role of the heavy-atom effect are now in progress, wherein not only the outer surface Zr^{4+} but also the inner bridging Zr^{4+} cations are replaced with heavier metal ions.

Conclusion

To promote the dye regeneration by the redox-reversible electron donor, we investigated the outer metal ion dependence of the photocatalytic H_2 evolution activity of DSP nanoparticles, X'-**RuCP^6**-Zr-**RuP^6**@Pt-TiO_2 (**X'-DSPs**). We found that not only the previously reported Zr^{4+} but also the other metal cations (Fe^{2+}, Y^{3+}, Hf^{4+}, and Bi^{3+}) were successfully immobilized onto the outer surface of the **RuCP^6**-Zr-**RuP^6**@Pt-TiO_2nanoparticle (**H^+-DSP**), whereas the labile cation Sr^{2+} was easily desorbed from the nanoparticle surface in the aqueous solution. These results suggest that metal cations with small hydration enthalpies are not suitable for the surface functionalization of the **H^+-DSP** nanoparticle photocatalyst. The AQY values of metal-cation-immobilized **X'-DSPs** at 460 nm in the presence of 0.5 M KI aqueous solution were in the range 0.47–0.61%, which are higher than that of **H^+-DSP** (AQY = 0.302%). This suggests that the surface metal cations act as the attracting site to promote the electron donation from iodide mediator. Although not only I^- but also the oxidative byproduct I_3^- could be also attracted by the surface metal cations, the charge recombination between the surface attracted I_3^- and electron injected $TiO_2(e^-)$ could be suppressed by the thick doubly-layered Ru(II) dyes.[52,53] On the other hand, **Bi^{3+}-DSP** and **Fe^{2+}-DSP**, which comprise redox-active outer metal ions, showed slightly lower photocatalytic activity than the photocatalysts with redox-inactive outer metal cations (**X'-DSPs**, X' = Zr^{4+}, Hf^{4+}, and Y^{3+}), possibly because of the reverse electron transfer from the photoexcited Ru dye to the outer metal cations. We also observed that **Zr^{4+}-DSP**, **Hf^{4+}-DSP**, and **Bi^{3+}-DSP** can drive the photocatalytic H_2 evolution reaction with 0.2–0.3% AQY under green light illumination at 530 nm, which is located in the absorption band edge of Ru PSs. Further studies to reveal the role of crosslinked Zr cations in interlayer energy/electron transfer processes by substituting the Zr cations with other metal cations are now in progress.

ASSOCIATED CONTENT

Supporting Information. Experimental details of the Ru(II) dye immobilized on the Pt-TiO_2 nanoparticles; UV-vis absorption spectra of all supernatant solutions obtained from the syntheses of Ru(II)-dye-immobilized Pt-TiO_2; XRF spectra of **Sr^{2+}-DSP** after immersion in 0.5 M KCl aq.; molar ratios of Zr/Ru and X'/Ru estimated by XRF analysis; UV-vis absorption spectra of the reaction solution of **Zr^{4+}-** and **Hf^{4+}-DSPs** after 6 h irradiation; SEM-EDS analysis for **Hf^{4+}-DSP** before and after 6 h irradiation; photocatalytic H_2 evolution by **Hf^{4+}-DSP** under green light irradiation for 20 h; and zeta potentials and UV-vis diffuse reflectance spectra of **X'-DSPs** (PDF). This material is available free of charge on the Internet at http://pubs.acs.org.

AUTHOR INFORMATION

Corresponding Author

*E-mail: akoba@sci.hokudai.ac.jp (A.K.).

Author Contributions

The manuscript was written through the contributions of all authors. All the authors approved the final version of the manuscript.

Funding Sources

This study was supported by the ENEOS Hydrogen Trust Fund, Casio Science Promotion Foundation, JSPS KAKENHI, and Hokkaido University DX Doctoral Fellowship (grant numbers JP18K19086, JP17H06367, JP20H05082, and JPMJSP2119).

REFERENCES

(1) Acharya, S.; Padhi, D. K.; Parida, K. M. Visible Light Driven $LaFeO_3$ Nano Sphere/RGO Composite Photocatalysts for Efficient Water Decomposition Reaction. *Catal. Today* **2020**, *353*, 220–231.

(2) Graetzel, M. Artificial Photosynthesis: Water Cleavage into Hydrogen and Oxygen by Visible Light. *Acc. Chem. Res*. **1981**, *14*, 376–384.

(3) Ma, Y.; Wang, X.; Jia, Y.; Chen, X.; Han, H.; Li, C. Titanium Dioxide-Based Nanomaterials for Photocatalytic Fuel Generations. *Chem. Rev*. **2014**, *114*, 9987–10043.

(4) Kudo, A.; Miseki, Y. Heterogeneous Photocatalyst Materials for Water Splitting. *Chem. Soc. Rev.* **2009**, *38*, 253–278.

(5) Fang, X.; Kalathil, S.; Reisner, E. Semi-Biological Approaches to Solar-to-Chemical Conversion. *Chem. Soc. Rev.* **2020**, *49*, 4926–4952.

(6) Fujishima, A.; Honda, K. Electrochemical Photolysis of Water at a Semiconductor Electrode, *Nature* **1972**, *238*, 37–38.

(7) Ma, G.; Chen, S.; Kuang, Y.; Akiyama, S.; Hisatomi, T.; Nakabayashi, M.; Shibata, N.; Katayama, M.; Minegishi, T.; Domen, K. Visible Light-Driven Z-Scheme Water Splitting Using Oxysulfide H_2 Evolution Photocatalysts. *J. Phys. Chem. Lett.* **2016**, *7*, 3892–3896.

(8) Nakada, A.; Nishioka, S.; Vequizo, J. J. M.; Muraoka, K.; Kanazawa, T.; Yamakata, A.; Nozawa, S.; Kumagai, H.; Adachi, S.; Ishitani, O.; Maeda, K. Solar-Driven Z-Scheme Water

Splitting Using Tantalum/Nitrogen Co-Doped Rutile titania Nanorod as an Oxygen Evolution Photocatalyst. *J. Mater. Chem. A* **2017**, *5*, 11710–11719.

(9) Fang, M. J.; Tsao, C. W.; Hsu, Y. J. Semiconductor Nanoheterostructures for Photoconversion Applications. *J. Phys. D: Appl. Phys.* **2020**, *53*, 143001–143033.

(10) Kumagai, H.; Aoyagi, R.; Kato, K.; Yamakata, A.; Kakihata, M.; Kato, H. Utilization of Perovskite-Type Oxynitride $La_{0.5}Sr_{0.5}Ta_{0.5}Ti_{0.5}O_2N$ as an O_2-Evolving Photocatalyst in Z-Scheme Water Splitting. *ACS Appl. Energy Mater.* **2021**, 2056–2060.

(11) Wang, Q.; Hisatomi, T.; Jia, Q. X.; Tokudome, H.; Zhong, M.; Wang, C. Z.; Pan, Z. H.; Takata, T.; Nakabayashi, M.; Shibata, N.; Li, Y. B.; Sharp, I. D.; Kudo, A.; Yamada, T.; Domen, K. Scalable Water Splitting on Particulate Photocatalyst Sheets with a Solar-to-Hydrogen Energy Conversion Efficiency Exceeding 1%. *Nat. Mater.* **2016**, *15,* 611–615.

(12) Zhao, Y.; Liu, T.; Chen, R.; Zeng, B.; Tao, X.; Li, J.; Jin, X.; Li, R.; Li, C. Embedding Sulfur Atoms in Decahedron Bismuth Vanadate Crystals with a Soft Chemical Approach for Expanding the Light Absorption Range. *ChemCatChem* **2020**, *12*, 1585–1590.

(13) Duong, H. P.; Mashiyama, T.; Kobayashi, M.; Iwase, A.; Kudo, A.; Asakura, Y.; Yin, S.; Kakihana, M.; Kato, H. Z-scheme water splitting by microspherical Rh-doped $SrTiO_3$ photocatalysts prepared by a spray drying method. *Appl. Catal. B* **2019**, *252*, 222–229.

(14) Zhou, C.; Wang, S.; Zhao, Z.; Shi, Z.; Yan, S.; Zou, Z. A Facet-Dependent Schottky-Junction Electron Shuttle in a $BiVO_4${010}–Au–Cu_2O Z-Scheme Photocatalyst for Efficient Charge Separation. *Adv. Funct. Mater.* **2018**, *28*, 1801214.

(15) Li, X.; Yu, J.; Low, J.; Fang, Y.; Xiao, J.; Chen, X. Engineering heterogeneous semiconductors for solar water splitting. *J. Mater. Chem. A,* **2015**, *3*, 2485-2534.

(16) Stolarczyk, J. K.; Bhattacharyya, S.; Polavarapu, L.; Feldmann, J. Challenges and Prospects in Solar Water Splitting and CO_2 Reduction with Inorganic and Hybrid Nanostructures *ACS Catal.*, **2018**, *8*, 3602-3635.

(17) Nakada, A.; Uchiyama, T.; Kawakami, N.; Sahara, G.; Nishioka, S.; Kamata, R.; Kumagai, H.; Ishitani, O.; Uchimoto, Y.; Maeda, K. Solar Water Oxidation by Visible-Light-Responsive Tanta-lum/Nitrogen-Codoped Rutile TiO_2 Anode for Photoelectrochemical Overall Water Splitting and CO_2 Fixation. *ChemPhotoChem* **2019**, *3*, 37–45.

(18) Sheridan, M. V.; Wang, Y.; Wang, D.; Troian-Gautier, L. T.; Dares, C. J.; Sherman, B. D.; Meyer, T. J. Light-Driven Water Splitting Mediated by Photogenerated Bromine. *Angew. Chem. Int. Ed. Engl.* **2018**, *57*, 3449–3453.

(19) Warnan, J.; Willkomm, J.; Ng, J. N.; Godin, R.; Prantl, S.; Durrant, J. R.; Reisner, E. Solar H_2 Evolution in Water with Modified Diketopyrrolopyrrole Dyes Immobilized on Molecular Co and Ni Catalyst–TiO_2 Hybrids. *Chem. Sci*. **2017**, *8*, 3070–3079.

(20) Wang, X.; Chen, L.; Chong, S. Y.; Little, M. A.; Wu, Y.; Zhu, W. H.; Clowes, R.; Yan, Y.; Zwijnenburg, M. A.; Sprick, R. S.; Cooper, A. I. Sulfone-Containing Covalent Organic Frameworks for Photocatalytic Hydrogen Evolution from Water. *Nat. Chem*. **2018**, *10*, 1180–1189.

(21) Gueret, R.; Poulard, L.; Oshinowo, M.; Chauvin, J.; Dah-mane, M.; Dupeyre, G.; Lainé, P. P.; Fortage, J.; Collomb, M. Challenging the $[Ru(bpy)_3]^{2+}$ Photosensitizer with a

Triazatriangulenium Robust Organic Dye for Visible-Light-Driven Hydrogen Production in Water. *ACS Catal*. **2018**, *8*, 3792–3802.

(22) Guo, S.; Chen, K.; Dong, R.; Zhang, Z.; Zhao, J.; Lu, T. Robust and Long-Lived Excited State Ru(II) Polyimine Photosensitizers Boost Hydrogen Production. *ACS Catal*. **2018**, *8*, 8659–8670.

(23) Da Silva, E. S. D.; Moura, N. M. M.; Neves, M. G. P. M. S.; Coutinho, A.; Prieto, M.; Silva, C. G.; Faria, J. L. Novel Hybrids of Graphitic Carbon Nitride Sensitized with Free-Base meso-tetrakis(carboxyphenyl) Porphyrins for Efficient Visible Light Photo-catalytic Hydrogen Production. *Appl. Catal. B* **2018**, *221*, 56–69.

(24) Tsukamoto, T.; Takada, K.; Sakamoto, R.; Matsuoka, R.; Toyoda, R.; Maeda, H.; Yagi, T.; Nishikawa, M.; Shinjo, N.; Amano, S.; Iokawa, T.; Ishibashi, N.; Oi, T.; Kanayama, K.; Kinugawa, R.; Koda, Y.; Komura, T.; Nakajima, S.; Fukuyama, R.; Fuse, N.; Mizui, M.; Miyasaki, M.; Yamashita, Y.; Yamada, K.; Zhang, W.; Han, R.; Liu, W.; Tsubomura, T.; Nishihara, H. Coordination Nanosheets Based on Terpyridine-Zinc(II) Complexes: As Photoactive Host Materials. *J. Am. Chem. Soc*. **2017**, *139*, 5359–5366.

(25) Lee, J. S.; Won, D. I.; Jung, W. J.; Son, H. J.; Pac, C.; Kang, S. O. Widely Controllable Syngas Production by a Dye-Sensitized TiO_2 Hybrid System with Re^{I} and Co^{III} Catalysts under Visible-Light Irradiation. *Angew. Chem. Int. Ed. Engl*. **2017**, *56*, 976–980.

(26) Aslan, E.; Gonce, M. K.; Yigit, M. Z.; Sarilmaz, A.; Statha-tos, E.; Ozel, F.; Can, M.; Patir, I. H. Photocatalytic H_2 Evolution with a Cu_2WS_4 Catalyst on a Metal freeD-π-A Organic Dye-Sensitized TiO_2. *Appl. Catal. B* **2017**, *220*, 320–327.

(27) Tiwari, A.; Krishna, N. V.; Giribabu, L.; Pal, U. Hierarchical Porous TiO_2 Embedded Unsymmetrical Zinc–Phthalocyanine Sensitizer for Visible-Light-Induced Photocatalytic H_2 Production. *J. Phys. Chem. C* **2018**, *122*, 495–502.

(28) Yu, F.; Cui, S.; Li, X.; Peng, Y.; Yu, Y.; Yun, K.; Zhang, S.; Li, J.; Liu, J.; Hua, J. Effect of Anchoring Groups on N-Annulated Perylene-Based Sensitizersfor Dye-Sensitized Solar Cells and Photo-catalytic H_2 Evolution. *Dyes Pigm.* **2017**, *139*, 7–18.

(29) Sun, Y.; Sun, Y.; Dall'Agnese, C.; Wang, X.; Chen, G.; Kitao, O.; Tamiaki, H.; Sakai, K.; Ikeuchi, T.; Sasaki, S. Dyad Sensitizer of Chlorophyll with Indoline Dye for Panchromatic Photocatalytic Hydrogen Evolution. *ACS Appl. Energy Mater.* **2018**, *1*, 2813–2820.

(30) R. Abe, K. Shinmei, N. Koumura, K. Hara, B. Ohtani, Visible-Light-Induced Water Splitting Based on Two-Step Photoexcitation between Dye-Sensitized Layered Niobate and Tungsten Oxide Photocatalysts in the Presence of a Triiodide/Iodide Shuttle Redox Mediator. *J. Am. Chem. Soc*., **2013**, *135*, 16872-16884.

(31) Oshima, T.; Nishioka, S.; Kikuchi, Y.; Hirai, S.; Yanagisawa, K. I.; Eguchi, M.; Miseki, Y.; Yokoi, T.; Yui, T.; Kimoto, K.; Sayama, K.; Ishitani, O.; Mallouk, T. E.; Maeda, K. An Artificial Z-Scheme Constructed from Dye-Sensitized Metal Oxide Nanosheets for Visible Light-Driven Overall Water Splitting. *J. Am. Chem. Soc.* **2020**, *142*, 8412–8420.

(32) Tosco, B.; Melo, B. P. V.; Merino, D. H.; Rey, J. F. Q.; Brochsztain, S. Layer-by-Layer Naphthalenediimide/Zn Phosphonate Hybrid Films Grown from Aqueous Solutions by a Simple Deposition Technique. *Langmuir,* **2011**, *37*, 2494–2502.

(33) Beauvilliers, E. E.; Meyer, G. J. Evidence for Cation-Controlled Excited-State Localization in a Ruthenium Polypyridyl Compound. *Inorg. Chem.,* **2016**, *55*, 7517–7526.

(34) Wang, J. C.; Hill, S. P.; Dilbeck, T.; Ogunsolu, O. O.; Banerjee, T.; Hanson, K. Multimolecular assemblies on high surface areametal oxides and their role in interfacial energy and electron transfer. *Chem. Soc. Rev.*, **2018**, *47*, 104–148.

(35) Freitag, M.; Galoppini, E. Molecular host–guest complexes: Shielding of guests on semiconductor surfaces. *Energy Environ. Sci.*, **2011**, *4*, 2482–2494.

(36) Hanson, K.; Torelli, D. A.; Vannucci, A. K.; Brennaman, K.; Luo, H.; Alibabaei, L.; Song, W.; Ashford, D. L.; Norris, M. R.; Glasson, C. R. K.; Concenpcion, J. J.; Meyer, T. J. Self-Assembled Bilayer Films of Ruthenium(II)/Polypyridyl Complexes through Layer-by-Layer Deposition on Nanostructured Metal Oxides. *Angew. Chem.,* **2012**, *124*, 12954–12957.

(37) Ma, D.; Bettis, S. E.; Hanson, K.; Minakova, M.; Alibabaei, L.; Fondrie, W.; Ryan, D. K.; Papoian, G. A.; Meyer, T. J.; Waters, M. L.; Papanikolas, J. M. Interfacial Energy Conversion in RuII Polypyridyl-Derivatized Oligoproline Assemblies on TiO_2. *J. Am. Chem. Soc*. **2013**, *135*, 5250–5253.

(38) Ogunsolu, O. O.; Murphy, I. A.; Wang, J. C.; Das, A.; Hanson, K. Energy and Electron Transfer Cascade in Self-Assembled Bilayer Dye-Sensitized Solar Cells. *ACS Appl. Mater. Interfaces* **2016**, *8*, 28633–28640.

(39) Ogunsolu, O. O.; Wang, J. C.; Hanson, K. Increasing the Open-Circuit Voltage of Dye-Sensitized Solar Cells via Metal-Ion Coordination. *Inorg. Chem*. **2017**, *56*, 11168–11175.

(40) Ogunsolu, O. O.; Braun, A. J.; Robb, A. J.; Salpage, S. R.; Zhou, Y.; Hanson, K. Influence of Dye-Coordinated Metal Ions on Electron Transfer Dynamics at Dye–Semiconductor Interfaces. *ACS Appl. Energy Mater*. **2019**, *2*, 29–36.

(41) Wang, J. C.; Violettem K.; Ogunsolu, O. O.; Cekli, S.; Lambers, E.; Fares, H. M.; Hanson, K. Self-Assembled Bilayers on Nanocrystalline Metal Oxides: Exploring the Non-Innocent Nature of the Linking Ions. *Langmuir* **2017**, *33*, 9609–9619.

(42) Wang, J. C.; Violette, K.; Ogunsolu, O. O.; Hanson, K. Metal ion mediated electron transfer at dye–semiconductor interfaces, *Phys. Chem. Chem. Phys.* **2017**, *19*, 2679-2682.

(43) Wang, J. C.; Ogunsolu, O. O.; Sykora, M.; Hanson, K. Elucidating the Role of the Metal Linking Ion on the Excited State Dynamics of Self-Assembled Bilayers. *J. Phys. Chem. C* **2018**, *122*, 9835–9842.

(44) Zhou, Y.; Ruchlin, C.; Robb, A. J.; Hanson, K. Singlet Sensitization-Enhanced Upconversion Solar Cells via Self-Assembled Trilayers. *ACS Energy Lett.* **2019**, *4*, 1458–1463.

(45) Kroeze, J. E.; Hirata, N.; Koops, S.; Nazeeruddin, Md. K.; Schmidt-Mende, L.; Grätzel, M.; Durrant, J. R. Alkyl Chain Barriers for Kinetic Optimization in Dye-Sensitized Solar Cells. *J. Am. Chem. Soc.* **2006**, *128*, 16376–16383.

(46) Pagba, C.; Zordan, G.; Galoppini, E.; Piatnitski, E. L.; Hore, S.; Deshayes, K.; Piotrowiak, P. Hybrid Photoactive Assemblies: Electron Injection from Host−Guest Complexes into Semiconductor Nanoparticles. *J. Am. Chem. Soc.* **2004**, *126*, 9888–9889.

(47) Choi, H.; Kang, S. O.; Ko, J.; Gao, G.; Kang, H. S.; Kang, M. Nazeeruddin, Md. K. Grätzel, M. An Efficient Dye-Sensitized Solar Cell with an Organic Sensitizer Encapsulated in a Cyclodextrin Cavity. *Angew. Chem., Int. Ed*., **2009**, *48*, 5938–5941.

(48) Freitag, M.; Galoppini, Cucurbituril Complexes of Viologens Bound to TiO_2 Films *Langmuir*, **2010**, *26*, 8282–8269.

(49) Li, H.; Li, F.; Wang, Y.; Bai, L.; Yu, F.; Sun, L. Visible-Light-Driven Water Oxidation on a Photoanode by Supramolecular Assembly of Photosensitizer and Catalyst. *ChemPlusChem*, **2016**, *81*, 1056–1059.

(50) Furugori, S.; Kobayashi, A; Watanabe, A.; Yoshida, M.; Kato, M. Impact of Photosensitizing Multi-layered structure on Ruthenium(II)-dye-sensitized TiO_2-nanoparticle Photocatalysts, *ACS Omega*, **2017**, *2*, 3901–3912.

(51) Yoshimura, N.; Kobayashi, A.; Yoshida, M.; Kato, M. A Systematic Study on the Double-Layered Photosensitizing Dye Structure on the Surface of Pt-Cocatalyst-Loaded TiO_2 Nanoparticles. *Bull. Chem. Soc. Jpn.* **2019**, *92*, 1793–1800.

(52) Yoshimura, N.; Kobayashi, A.; Genno, W.; Okubo, T.; Yoshida, M.; Kato, M. Photosensitizing Ruthenium(II)-Dye Multilayers: Photoinduced Charge Separation and Back Electron Transfer Suppression. *Sustain. Energy Fuels* **2020**, *4*, 3450–3457.

(53) Yoshimura, N.; Kobayashi, A.; Yoshida, M.; Kato, M. Enhancement of Photocatalytic Activity for Hydrogen Production by Surface Modification of Pt-TiO_2 Nanoparticles with a Double Layer of Photosensitizers. *Chem. Eur. J.* **2020**, *26*, 16939–16946.

(54) Yoshimura, N.; Kobayashi, A.; Kondo, T.; Abe, R.; Yoshida, M.; Kato, M. Interfacial Electron Flow Control by Double Nano-architectures for Efficient Ru-dye-sensitized Hydrogen Evolution from Water. *ACS Appl. Energy Mater.*, **2021**, *4*, 14352-14362.

(55) Li, X.; Nazeeruddin, M. K.; Thelakkat, M.; Barnes, P. R. F.; Vilar, R.; Durrant, J. R. Spectroelectrochemical Studies of Hole Percolation on Functionalized Nanocrystalline TiO_2 Films: a Comparison of Two Different Ruthenium Complexes, *Phys. Chem. Chem. Phys.* **2011**, *13*, 1575-1584.

(56) Park, H.; Choi, W.; Hoffmann, M. R. Effects of the preparation method of the ternary CdS/TiO_2/Pt hybrid photocatalysts on visible light-induced hydrogen production. *J. Mater. Chem.* **2008**, *18*, 2379-2385.

(57) Hanson, K.; Brennaman, M. K.; Ito, A.; Luo, H.; Song, W.; Parker, K. A.; Ghosh, R.; Norris, M. R.; Glasson, C. R. K.; Concepcion, J. J.; Lopez, R.; Meyer, T. J. Structure−Property Relationships in Phosphonate-Derivatized, Ru^{II} Polypyridyl Dyes on Metal Oxide Surfaces in an Aqueous Environment. *J. Phys. Chem. C* **2012**, *116*, 14837–14847.

(58) Troian-Gautier, L.; Turlington, M. D.; Wehlin, S. A. M.; Maurer, A. B.; Brady, M. D.; Swords, W. B.; Meyer, G. J. Halide Photoredox Chemistry. *Chem. Rev.* **2019**, *119*, 4628–4683.

(59) Troian-Gautier, L.; Swords, W. B.; Meyer, G. J. Iodide Photoredox and Bond Formation Chemistry. *Acc. Chem. Res.* **2019**, *52*, 170–179.

For Table of Contents Only

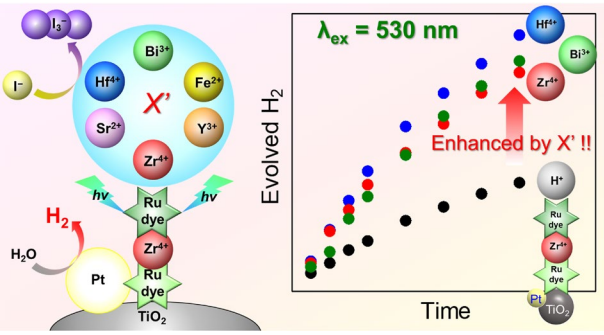

To improve the reactivity between photosensitizer and electron mediator in photo water splitting reaction, we synthesized an X'-**RuCP^6**–Zr-**RuP^6**@Pt-TiO_2 (**X'-DSPs**) series composed of Pt-cocatalyst-loaded TiO_2 nanoparticles, sensitized by a double layer of Ru(II) dyes with different surface-bound metal cations. We found that metal-cation-immobilized **X'-DSPs** exhibited 1.5–2-fold higher apparent quantum yields in 0.5 KI aqueous solution under green light than **H$^+$-DSP**.